Composites Science and Technology 69 (2009) 1180–1186

Contents lists available at ScienceDirect

Composites Science and Technology

journal homepage: www.elsevier.com/locate/compscitech

In situ probe nanophase transition in nanocomposite using thermal AFM

Chien-Chih Lin [a], Kuo-Hsin Chang [b], Keng-Ching Lin [c], Wei-Fang Su [a,b,*]

[a] Institute of Polymer Science and Engineering, National Taiwan University, No. 1, Sec. 4, Roosevelt Road, Taipei 10617, Taiwan
[b] Institute of Materials Science and Engineering, National Taiwan University, No. 1, Sec. 4, Roosevelt Road, Taipei 10617, Taiwan
[c] Department of Physics, FuJen Catholic University, No. 510, Chung Cheng Road, Hsinchuang, Taipei County 24205, Taiwan

ARTICLE INFO

Article history:
Received 13 March 2008
Received in revised form 12 September 2008
Accepted 12 February 2009
Available online 20 February 2009

Keywords:
A. Nanocomposites
A. Nanoparticles
B. Mechanical properties
B. Thermal properties
D. Atomic force microscopy (AFM)

ABSTRACT

Nanocomposites made from inorganic nanoparticles and polymers have many applications in optics, electronics and biomaterials. However, the glass transition temperature (T_g) of a nanocomposite is very difficult to measure accurately by conventional thermal analysis such as DSC or TMA when the concentration of the nanoparticle reaches a threshold of the percolation network. At this threshold stage, the phase transition in the nano domains of the matrix is too small to be detected by macroscale thermal analysis. We have developed a methodology basis on thermal atomic force microscope (AFM) to monitor the nanophase transition of the nanocomposite in situ upon heating. This method has demonstrated the capability in determining the T_g of a nanocomposite made by spherical SiO_2 nanoparticles dispersed in polyacrylate. The threshold of the percolation network of this nanocomposite is at 40 wt% of SiO_2 nanoparticles according to the results of refractive index, AFM, nanoindentation, DSC, TMA and TGA.

1. Introduction

While polymers are light weighted, conformable, flexible, and easy to process, they remain relatively poor in thermal, mechanical, optical and electronic performance. On the other hand, inorganic materials usually exhibit good physical properties but are heavy, rigid and difficult to process. By nanosizing an inorganic material and dispersing it into a polymer to make nanocomposite [1–3], it is possible to utilize the merits of both materials. Thus, nanocomposites can be used in wide applications such as thin film [4], optics [5], waveguide [6], light emitting diode [7], solar cell [8,9], biomimic material [10–12] and so on.

The spatial distribution and the interface characteristics of individual constituents within the composite affect its physical nature including optical [4,5], electronic [7,8], thermal [13–17] and mechanical properties [18–24]. There are various studies targeted at establishing the connection among macroscopic behaviors, micro-structures and nano-structures from both theoretical and experimental approaches [25,26]. The encapsulated nanoparticles within polymers would eventually form a percolated network within the composite. The rigid backbone formed by the nanoparticles in polymer phase reinforces the nanocomposite and causes an increase in both mechanical strength [2,12,26] and thermal properties [4,5,10,11,28]. Buxton and Balazs [26] simulation results show that the nanoparticles are confined within a close proximity of each other and that long range order has been suppressed due to the winding polymer domains. With higher nanoparticle volume fractions, there is an increased effect of distribution on the relative strain within the nanocomposites. The elastic modulus is predicted to be increased nonlinearly as the nanoparticle composition increases. We have carried out a systematic study for a SiO_2–polyacrylate nanocomposite system with the concentration of SiO_2 ranging from 10 wt% to 60 wt%. The nonlinear relationship between properties and composition of the nanocomposite was observed for optical property, mechanical strength and thermal behaviors.

AFM is a tool commonly used to image the surface topography and surface morphology of materials. However, most of the experiments probing the surface morphology with AFM instrument are conducted at room temperature. McMaster et al. [29] observed the growth of lamellae structure with AFM at room temperatures but most polymers have phase transitions above room temperature. Others have [30,31] tried to use AFM to observe composites at room temperature after heating them for variable times in advance. Hobbs [32] has carried out in situ AFM of polymer crystallization which differs from nanocomposite systems. Therefore, we have used the AFM equipped with thermal accessory (thermal AFM) in situ to probe nanophase transition in the nanocomposites which can not be observed using conventional thermal analysis equipment such as DSC and TMA.

* Corresponding author. Address: Institute of Polymer Science and Engineering, National Taiwan University, No. 1, Sec. 4, Roosevelt Road, Taipei 10617, Taiwan. Tel./fax: +886 2 3366 4078.
E-mail address: suwf@ntu.edu.tw (W.-F. Su).

0266-3538/$ - see front matter © 2009 Elsevier Ltd. All rights reserved.
doi:10.1016/j.compscitech.2009.02.017

Table 1
Compositions of SiO_2–polyacrylate nanocomposites in wt%.[a]

Samples	SiO_2	MPS	TEGDA	EOBDA
FS-0	0	0	70.00	30.00
FS-10	9.43	2.36	61.75	26.46
FS-20	18.87	4.72	53.49	22.92
FS-40	37.74	9.43	36.98	15.85
FS-50	47.17	11.79	28.73	12.31
FS-60	56.60	14.15	20.47	8.77

[a] 4 wt% of photo-initiator is used on the basis of the organic part of samples.

2. Experimental

2.1. Materials

MA-ST-M (20–25 nm, 40 wt% silica content, Nissan Chemistry), 3-(trimethoxysilyl) propyl methacrylate (MPS, 98%, ACROS), tetraethylene glycol diacrylate (TEGDA, TCI), ethoxylated bisphenol A diacrylate (EOBDA, SARTOMER), 2,2-dimethoxy-2-phenyl acetophenone (Irgacure 651, CIBA) and methanol (99.98%, TEDIA) were purchased and used without further purification.

2.2. Preparation of 20–25 nm surface modified SiO_2 nanoparticles solution

Surface modified silica nanoparticles solution was prepared by mixing 20 mL MA-ST-M colloidal solution with 20 mL methanol for 10 min first, then adding 2 mL MPS as coupling agent and reacted at 50 °C for 24 h.

2.3. Preparation of nanocomposite solutions

The compositions of the nanocomposite solution, labeled as a FS series, are listed in Table 1. The nanocomposite solution was prepared according to our established method [12]. The general procedure is by mixing the surface modified SiO_2 nanocomposite solution with a mixture of TEGDA and EOBDA and photo-initiator (Irgacure 651) in an Al-foil covered flask to shield it from light. The mixing is under constant stirring for 1 h at room temperature. Then, the solvent in the mixture was removed under vacuum ($\sim 10^{-3}$ torr) for about 1 h to make a solventless nanocomposite solution.

2.4. Preparation of nanocomposite samples

The about 1 μm nanocomposite film sample was prepared by spin-coating the above solution on silicon wafer at 6000 rpm for 60 s, then the wet film was cured by a UV light (365 nm, 1.86 mW/cm^2) for 2 min in a N_2 chamber, then post-cured at 100 °C for 12 h. The about 100 μm nanocomposite film sample was prepared by casting the solution in a PET mold, then cured by a UV light (365 nm, 1.86 mW/cm^2) for 2 min in a N_2 chamber. All the films thickness was measured by a surface profiler (Tencor instrument Alpha-step 500). The disk sample of 5 mm (diameter) × 2 mm (thick) was prepared by casting the solution in a Teflon mold, then cured by a UV light (365 nm, 1.86 mW/cm^2) for 5 min on both sides and post-cured at 100 °C for 12 h.

2.5. Characterization

The refractive index of the 100 μm nanocomposite film was measured using a prism coupler (Metricon 2010) and a laser beam at 633 nm from a He–Ne laser was used in this measurement.

The Vickers hardness test was performed on the disk samples with a UMIS II (Ultra-micro indentation system) pyramid-shaped indenter (CSIRO). The measurements were performed under the maximum force load of 5 mN.

The macroscale glass transition temperatures of the nanocomposite were measured in a nitrogen atmosphere at a heating rate of 5 °C/min from 0 to 150 °C using a TA instruments DSC-2910. The glass transition temperature and coefficient of thermal expansion of the nanocomposite were measured in a nitrogen atmosphere at a heating rate of 5 °C/min from 20 to 150 °C using a TA instruments TMA-2940. The thermal decomposition temperatures of the nanocomposite were measured in an air atmosphere at a heating rate of 10 °C/min from 50 to 800 °C using a TA instruments TGA-2950.

The nanoscale morphology and the glass transition temperature of spin-coated nanocomposite films were measured with the Multi-Mode Atomic Force Microscope, 5597 EV (Digital Instruments) equipped with heating accessory. Our measurements are done in tapping mode with silicon cantilevers coated with Al on its reflective side. Its resonant frequency and force constant are 325 kHz and 40 N/m, respectively. The detailed data analysis of AFM results is described in the following sections.

2.6. Image processing method for changing three-dimensional landscape AFM image into a black–white binary image

We have used image processing software [33] to change the AFM images into a binary image. The procedure is described as follows. The h-range (height) of the AFM measurement is set at 100 nm (Δh) as sketched in the graph (Scheme 1). In our system, morphology variation is greater than 15 nm due to the size of the nanoparticle (about 20 nm), so we use 15 nm to be our base threshold value to do the further image processing. The actual volume expansion is three-dimensional. The threshold value δh should be accountable for the z-variation. However, our methodology simplifies the volume growth and δh is a fixed value in our

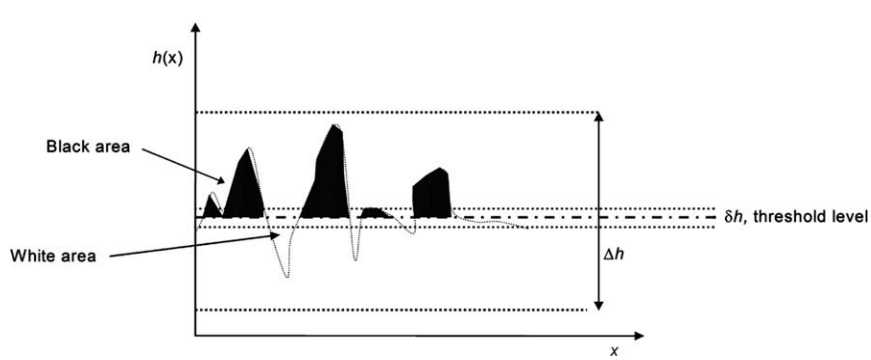

Scheme 1. Define the threshold level for converting AFM image into binary image.

analysis which would be canceled out when the area ratio is calculated. Then we can obtain the two-dimensional morphological images of AFM usually shown are the $h(x,y)$ functions. We define the threshold level at the mid-point of the fixed height range. Data points with value higher than the threshold level are set to be black and the points with value lower than the threshold level are set to be white. Thus, the three-dimensional landscape is converted into a black–white image. The mass flow through the threshold level is the volume change of protruded islands. Hence, the volume change can be expressed as:

$$d(volume) = d(area) \times \delta h \quad (1)$$

The δh is considered as a small but fixed value.

2.7. The determination of glass transition temperature from thermal AFM images

Furthermore, we can simplify Eqs. (1) and (2) as δh is a fixed value in our analysis. The volume change is in direct proportion as the area change can be expressed as:

$$d(volume) \propto d(area) \quad (2)$$

Relative to the thermal expansion, the polyacrylate is much easier than silica for the nanocomposites. We can assume the polyacrylate area will increase with rising temperature as the thermal AFM images are converted to black and white images. In other words, we can calculate the specific area fraction at the specific temperature by AFM measurement. By plotting the area fraction

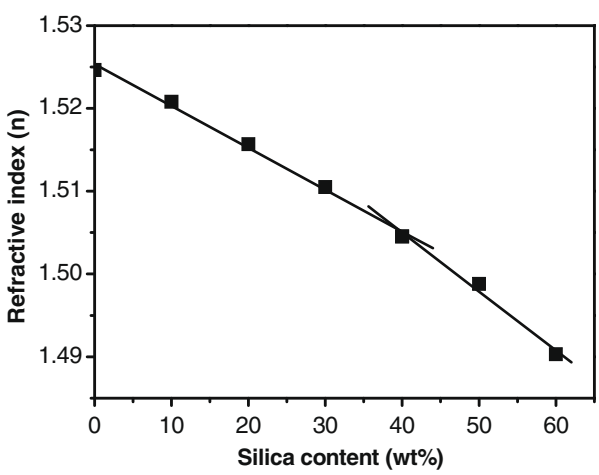

Fig. 1. Refractive index linear fit as a function of SiO_2 weight concentration at 633 nm.

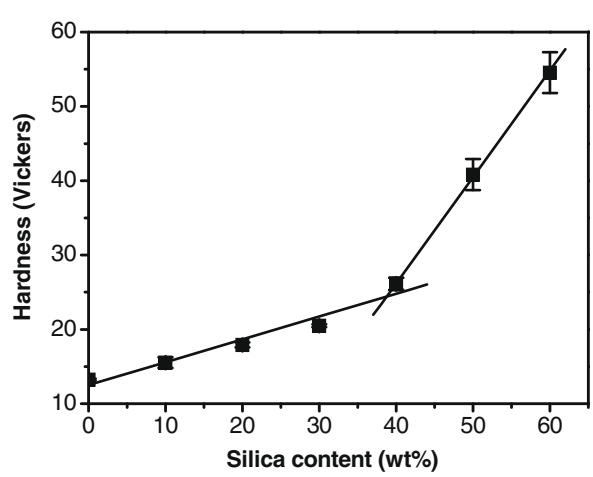

Fig. 2. The measured hardness linear fit as a function of SiO_2 weight concentration.

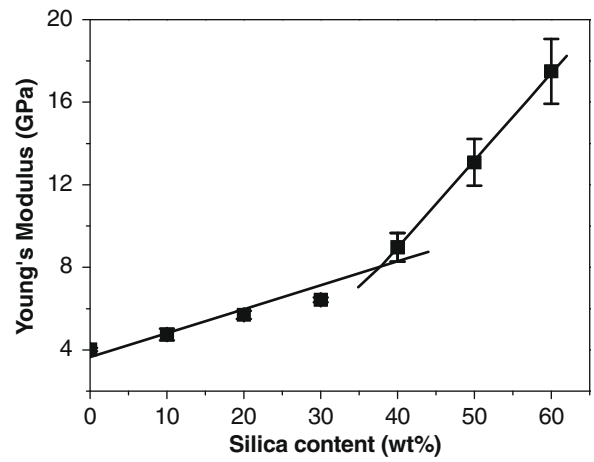

Fig. 3. The measured Young's modulus linear fit as a function of SiO_2 weight concentration.

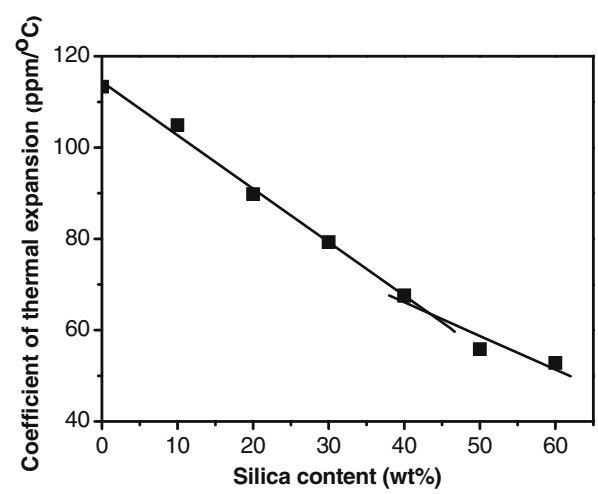

Fig. 4. Coefficient of thermal expansion linear fit as a function of SiO_2 weight concentration.

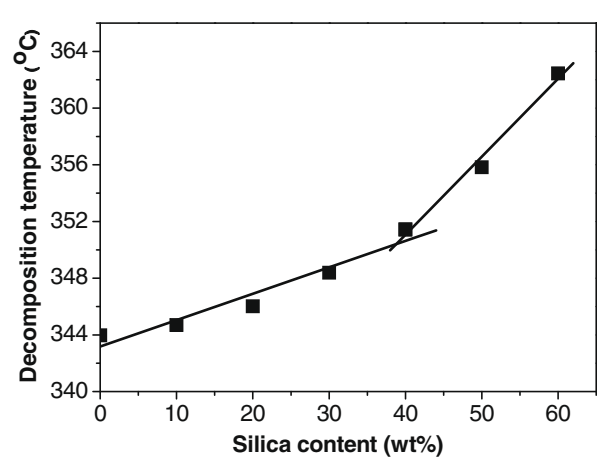

Fig. 5. Decomposition temperature linear fit as a function of SiO_2 weight concentration.

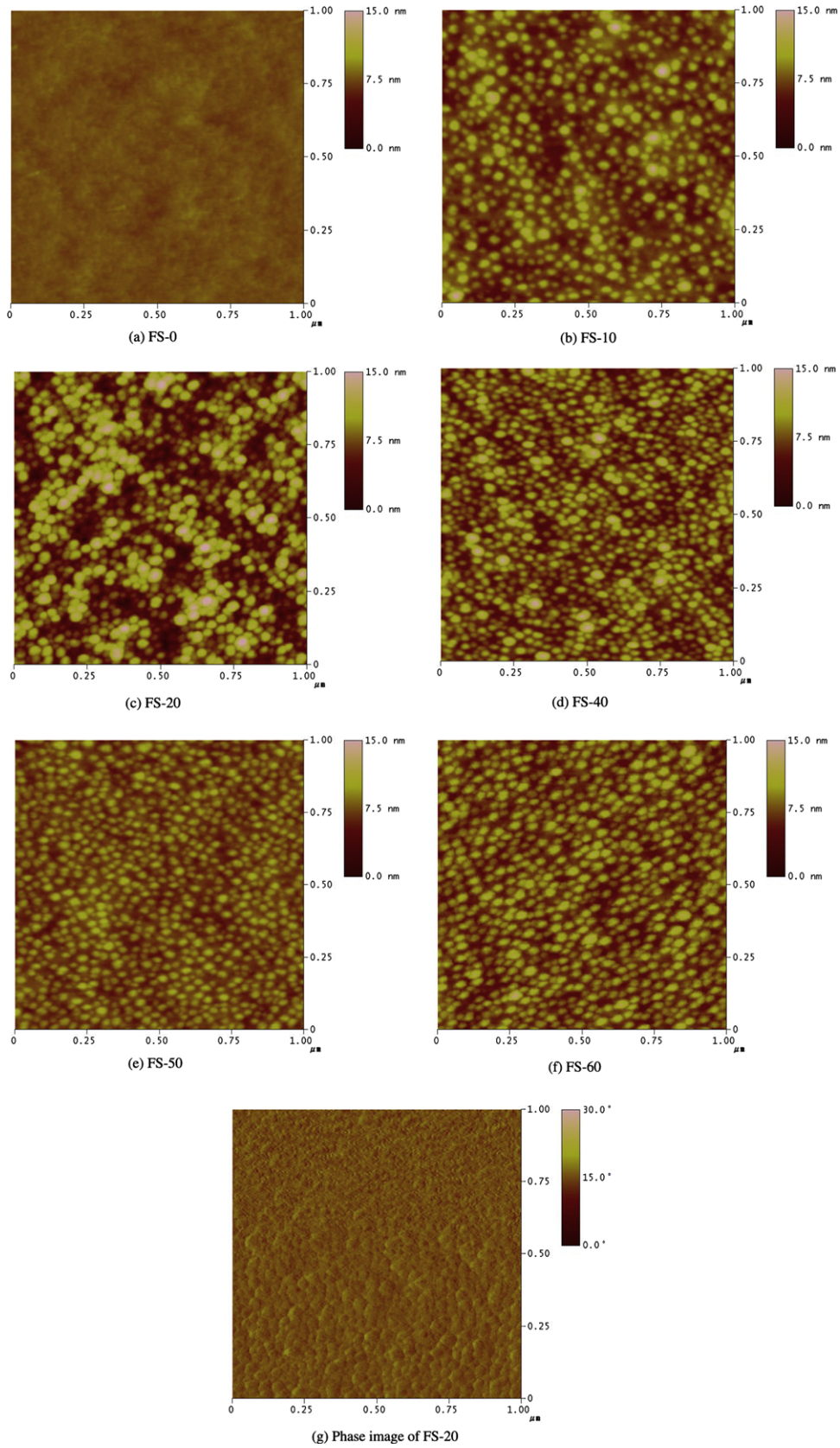

Fig. 6. AFM tapping mode images of samples: (a) FS-0, (b) FS-10, (c) FS-20, (d) FS-40, (e) FS-50, (f) FS-60 and (g) the phase image of FS-20 (scan size 1 μm × 1 μm, surface roughness scale in nm).

vs. temperature with linear fitting method, we can observe a dramatic change in slope easily. The change of the slope indicates the phase transition of the nanocomposites. By extrapolating two linear fitting lines to obtain an intersection, this intersection defines the T_g of the nanocomposites. Fig. 9 shows the results of FS-60 sample. We have used the same procedure to determine the T_g of FS-0, FS-20 and FS-40, respectively.

3. Results and discussion

We have synthesized SiO_2–polyacrylate nanocomposite for optical waveguide application. This material is designed to possess the properties of high optical transparency, tunable refractive index, high thermal stability and high elastic modulus. The polyacrylate is obtained by photo-polymerization of a mixture of tetraethylene glycol diacrylate (TEGDA) and ethoxylated bisphenol A diacrylate (EOBDA) monomers (70:30 by weight). The TEGDA is an aliphatic acrylate monomer that provides good optical properties and low viscosity for ease of processing [34]. The EOBDA contains aromatic moiety that provides good thermal stability [34]. The addition of SiO_2 nanoparticles into the nanocomposite is to adjust the refractive index of the material and to improve the thermal and mechanical properties of the material. The surface of SiO_2 nanoparticle was modified by 3-(trimethoxysilyl) propyl methacrylate (MPS) to be compatible with the acrylate matrix and to form 3D crosslinked interpenetrating network after polymerization. This is a solventless photo-polymerization system which is environmentally friendly and uses less energy as compared with solvent based thermal polymerization systems. Table 1 summarizes the compositions of samples that used in this study.

Fig. 1 shows the trend of the refractive indexes of the material decreasing with increasing SiO_2 concentrations with a bend at 40 wt% SiO_2. A similar nonlinear relationship is also observed for the mechanical properties and the thermal properties of the nanocomposite. Figs. 2 and 3 show the hardness and modulus of the material improves with an increase in SiO_2 concentrations. The extent of the improvement has a certain jump at the 40 wt% SiO_2 and continues to increase for higher concentrations. Similar results are observed in the studies of thermal expansion coefficient (Fig. 4) and thermal decomposition temperature (Fig. 5) of the material. We believe a close-packed arrangement of SiO_2 network is being built at the critical concentration of 40 wt%. This can be viewed as the percolation threshold of the system [2,26,27]. Upon reaching this threshold, the molecular movement for the polymer has been restricted by the nanoparticle network. Hence, an abnormally large increasing in physical properties is present.

We have used AFM to study the morphology of the nanocomposite with different compositions. Figs. 6a and b show the SiO_2 nanoparticles distributed randomly when the concentration of SiO_2 is less than 10 wt% in the nanocomposite. When the SiO_2 concentration increases to 20 wt%, the sample shows some aggregation (Fig. 6c). As the SiO_2 concentration reaches 40 wt%, the morphology appears to be arranged regularly (Fig. 6d), i.e. the nanocomposite has achieved percolation threshold at this time. 50 wt% (Fig. 6e) and 60 wt% (Fig. 6f) samples appear as almost close-packed surfaces. From Fig. 6g, phase image confirms SiO_2 nanoparticles are embedded in the polyacrylate matrix to form a nanocomposite film.

We have used image processing software [33] to change the AFM images into binary images as shown in Figs. 7a–d. The white

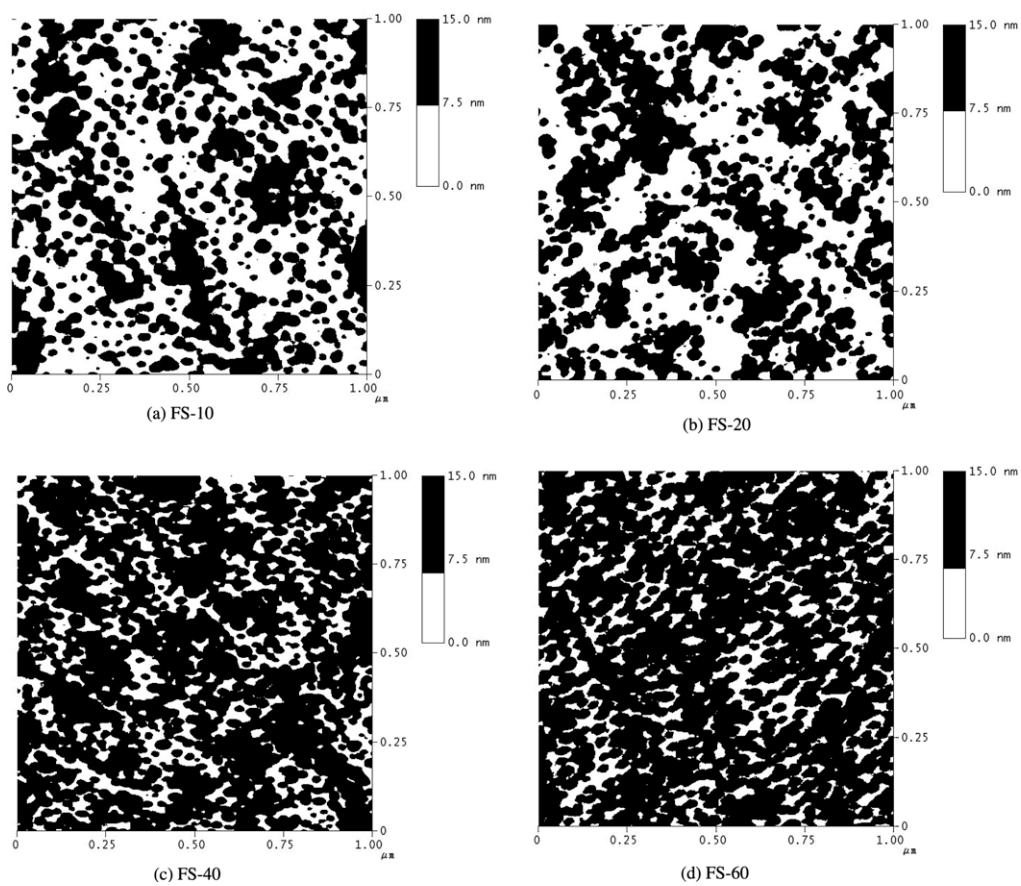

Fig. 7. The processed AFM images of FS series samples. Black area indicates the nanoparticles filling area and white area is assumed as the vacancy region. Possible percolation occurs after the nanoparticle content achieves a critical value for this network (scan size 1 μm × 1 μm).

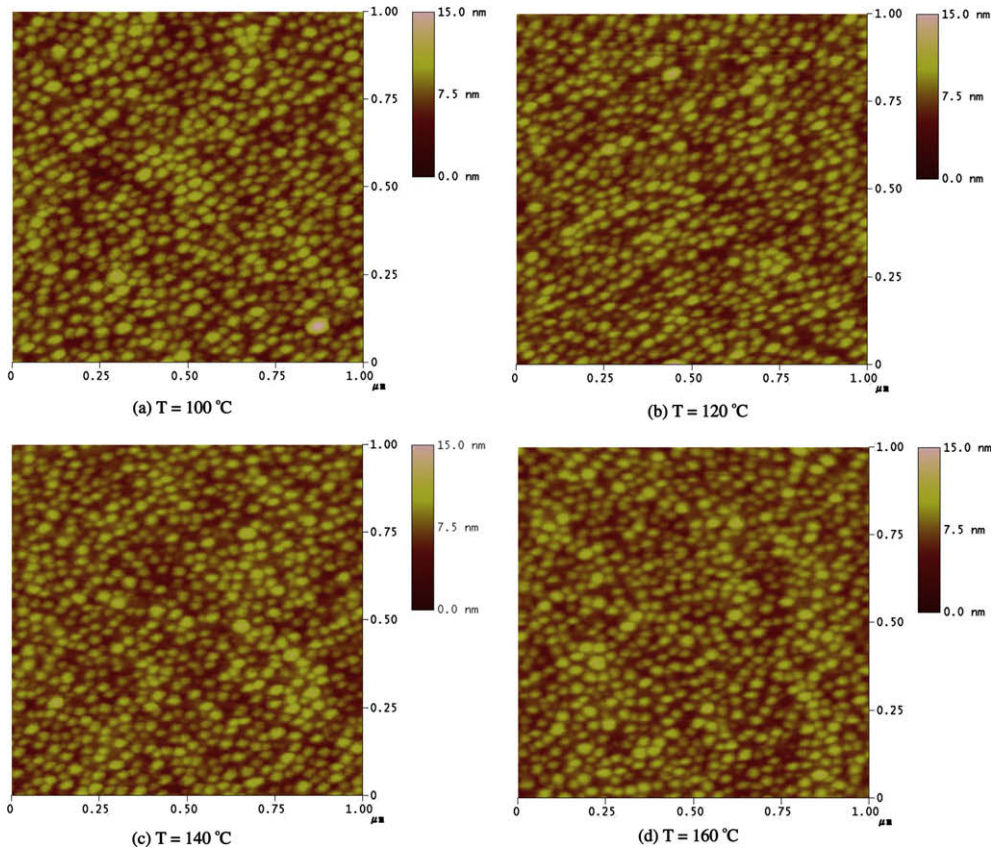

Fig. 8. Surface morphology of FS-60 at various temperatures (scan size 1 μm × 1 μm).

area is the polyacrylate matrix and the black area is the aggregate of SiO_2 nanoparticles. The black area clearly indicates the formation of percolation network of SiO_2 nanoparticles. The polyacrylate matrix is dispersed inside the network as nano domains. Furthermore, we have conducted more detailed studies of the threshold percolation network formation of SiO_2–polyacrylate system using small angle X-ray and TEM; these results will be published separately.

DSC and TMA cannot detect any glass transition of this nanocomposite when it contains more than 40 wt% SiO_2. The nano domains of the polyacrylate are too small to be detected by conventional macro scale measurement. We used thermal AFM to sense the phase changes of nano domains at elevated temperature as shown in Figs. 8a–d. Although the morphologies of the nanocomposite at different temperatures resemble each other, we can define a quantitative way to characterize them. Again, this was done using the image processing software to convert the thermal AFM images to black and white binary images and then calculate the percentage of polyacrylate area from the white area of the images. We assumed the polyacrylate area would increase with rising temperature due to the thermal expansion of polyacrylate. By plotting the percentage of polyacrylate vs. temperature, we have determined the T_g at the intersection of two linear extrapolations from the data as shown in Fig. 9.

All the glass transition T_g data measured by DSC, TMA and thermal AFM are summarized as in Table 2. We have found an interesting phenomenon in the nanocomposites FS-0 and FS-20 and T_g is about 42 °C and 51 °C, respectively, measured by thermal AFM, which is consistent to the results measured by DSC and TMA instruments. However, as the inorganic content achieves over 40 wt%, there is no distinct glass transition temperature (>150 °C) found by DSC and TMA while the T_g of such composition was clearly determined as 74 °C and 118 °C for FS-40 and FS-60, respectively, by thermal AFM. This result suggests that the nano domains of polymer in the nanocomposites still undergo phase transition

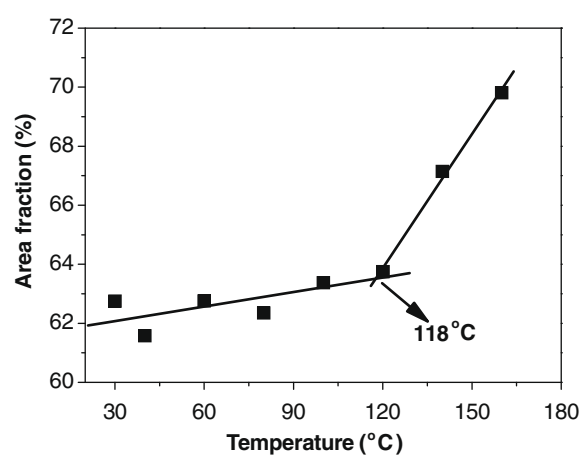

Fig. 9. Thermal evolution of the area fraction of FS-60. The solid lines are obtained by linear fit method.

Table 2
T_g comparison of FS series (DSC, TMA and AFM).

Samples	DSC, T_g (°C)	TMA, T_g (°C)	AFM, T_g (°C)
FS-0	42	43	44
FS-20	51	53	51
FS-40	>150	>150	74
FS-60	>150	>150	118

upon heating. The event is masked by the inorganic SiO_2 percolation network at macroscopic scale, but the nanosized probe of thermal AFM is sensitive enough to detect the nano domain phase transition in situ.

4. Conclusion

The optical, thermal and mechanical properties of silica–polyacrylate nanocomposites display a distinct transition when the silica content approaches 40 wt%. We have demonstrated experimentally by AFM measurements that there are corresponding structural transitions. This transition is due to the formation of the percolation network of silica nanoparticles within the polyacrylate matrix. Thermal AFM has been proven to be a useful tool in detecting nanophase transition in nanocomposites in situ.

Acknowledgements

Financial support obtained from the Ministry of Economic Affairs (93-EC-17-A-08-S1-0015) and National Science Council (NSC 95-3144-P-002-003-MY3) is highly appreciated. We also would like to thank Mr. An-Jey Su of University of Pittsburgh for editing the manuscript.

References

[1] Balazs AC, Emrick T, Russell TP. Nanoparticle polymer composites: where two small worlds meet. Science 2006;314(17):1107–10.
[2] Vaia RA, Giannelis EP. Polymer nanocomposites: status and opportunities. MRS Bull 2001;26:394–401.
[3] Winey KI, Vaia RA. Polymer nanocomposites. MRS Bull 2007;32:314–22.
[4] Su W-F, Lee J-F, Chen M-Y, Ho R-M. Bismuth titanate nanoparticles dispersed polyacrylates. J Mater Res 2004;19(8):2343–8.
[5] Nakayama N, Hayashi T. Preparation and characterization of TiO_2 and polymer nanocomposite films with high refractive index. J Appl Polym Sci 2007;105(6):3662–72.
[6] Park J-U, Kim W-S, Bae B-S. Photoinduced low refractive index in a photosensitive organic–inorganic hybrid material. J Mater Chem 2003;13:738–41.
[7] Lee C-Y, Huang Y-T, Su W-F, Lin C-F. Electroluminescence from ZnO nanoparticles/organic nanocomposites. Appl Phys Lett 2006;89:231116-1–6-3.
[8] Zeng T-W, Lin Y-Y, Lo H-H, Chen C-W, Chen C-H, Liou S-C, et al. A large interconnecting network within hybrid MEH-PPV/TiO_2 nanorod photovoltaic devices. Nanotechnology 2006;17:5387–92.
[9] Huynh WU, Dittmer JJ, Alivisatos AP. Hybrid nanorod-polymer solar cells. Science 2002;295:2425–7.
[10] Lin L-H, Liu H-J, Yu N-K. Morphology and thermal properties of poly(L-lactic acid)/organoclay nanocomposites. J Appl Polym Sci 2007;106:260–6.
[11] Pluta M, Jeszka JK, Boiteux G. Polylactide/montmorillonite nanocomposites: structure, dielectric, viscoelastic and thermal properties. Eur Polym J 2007;43:2819–35.
[12] Chen M-H, Chen C-R, Hsu S-H, Su W-F. Low shrinkage light curable nanocomposite for dental restorative material. Dent Mater 2006;22:138–45.
[13] Kashiwgai T, Morgan AB, Antonucci JM, VanLandingham MR, Harris RH, Awad WH, et al. Thermal and flammability properties of a silica–poly(methylmethacrylate) nanocomposite. J Appl Polym Sci 2003;89:2072–8.
[14] Chen Y, Zhou S, Yang H, Wu L. Structure and properties of polyurethane/nanosilica composites. J Appl Polym Sci 2005;95:1032–9.
[15] Kim JH, Ko JH, Bae BS. Dispersion of silica nano-particles in sol–gel hybrid resins for fabrication of multi-scale hybrid nanocomposite. J Sol–Gel Sci Technol 2007;41:249–55.
[16] Lee PI, Hsu SLC. Preparation and properties of polybenzoxazole–silica nanocomposites via sol–gel process. Eur Polym J 2007;43:294–9.
[17] Wang H, Xu P, Zhong W, Shen L, Du Q. Transparent poly(methyl methacrylate)/silica/zirconia nanocomposites with excellent thermal stabilities. Polym Degrad Stab 2005;87:319–27.
[18] Tyan HL, Liu YC, Wei KH. Thermally and mechanically enhanced clay/polyimide nanocomposite via reactive organoclay. Chem Mater 1999;11:1942–7.
[19] Wang Z, Pinnavaia TJ. Nanolayer reinforcement of elastomeric polyurethane. Chem Mater 1998;10:3769–71.
[20] Yang F, Nelson GL. PMMA/silica nanocomposite studies: synthesis and properties. J Appl Polym Sci 2004;91:3844–9.
[21] Jeon HS, Rameshwaram JK, Kim G, Weinkauf DH. Characterization of polyisoprene–clay nanocomposites prepared by solution blending. Polymer 2003;44:5749–58.
[22] Fisher FT, Brinson LC. Viscoelastic interphases in polymer–matrix composites: theoretical models and finite-element analysis. Compos Sci Technol 2001;61:731–48.
[23] Buryachenko VA, Roy A, Lafdi K, Anderson KL, Chellapilla S. Multi-scale mechanics of nanocomposites including interface: experimental and numerical investigation. Compos Sci Technol 2005;65:2435–65.
[24] Li C, Chou TW. Multi-scale modeling of compressive behavior of carbon nanotube/polymer composites. Compos Sci Technol 2006;66:2409–14.
[25] Paul DR, Bucknall CB. Polymer blends, vols. 1 and 2. New York: Wiley; 2000.
[26] Buxton GA, Balazs AC. Simulating the morphology and mechanical properties of filled diblock copolymers. Phys Rev E 2003;67:0318021–120.
[27] Yasmin A, Daniel IM. Mechanical and thermal properties of graphite platelet/epoxy composites. Polymer 2004;45:8211–9.
[28] Harada M, Minamigawa S, Tachibana K, Ochi M. Flame retardancy and thermomechanical properties of the poly(glycidyloxypropyl) phenyl silsesquioxane/layered titanate nanocomposites. J Appl Polym Sci 2007;106:338–44.
[29] McMaster TJ, Hobbs JK, Barham PJ, Miles M J. AFM study of in situ real time polymer crystallization and spherulite structure. Probe Microsc 1997;1:43–56.
[30] Ivanov DA, Jonas AM. Isothermal growth and reorganization upon heating of a single poly(aryl-ether-ether-ketone) (PEEK) spherulite, as imaged by atomic force microscopy. Macromolecules 1998;31:4546–50.
[31] Nuansing W, Ninmuang S, Jarernboon W, Maensiri S, Seraphin S. Structural characterization and morphology of electrospun TiO_2 nanofibers. Mater Sci Eng B 2006;131:147–55.
[32] Hobbs JK. In situ AFM of polymer crystallization. Chin J Polym Sci 2003;21:135–40.
[33] Russ JC. The image processing handbook. 3rd ed. Heidelberg (Germany)/Boca Raton (FL): Springer-Verlag/CRC Press; 1999.
[34] Stevens MP. Polymer chemistry: an introduction. 3rd ed. New York: Oxford University Press; 1999.